Lawrence Berkeley National Laboratory
LBL Publications

Title
Synthesis and x-ray characterization of sputtered bi-alkali antimonide photocathodes

Permalink
https://escholarship.org/uc/item/0d427913

Journal
APL Materials, 5(11)

ISSN
2166-532X

Authors
Gaowei, M
Ding, Z
Schubert, S
et al.

Publication Date
2017-11-01

DOI
10.1063/1.5010950

Peer reviewed

eScholarship.org Powered by the California Digital Library
University of California

Synthesis and x-ray characterization of sputtered bi-alkali antimonide photocathodes

M. Gaowei, Z. Ding, S. Schubert, H. B. Bhandari, J. Sinsheimer, J. Kuehn, V. V. Nagarkar, M. S. J. Marshall, J. Walsh, E. M. Muller, K. Attenkofer, H. J. Frisch, H. Padmore, and J. Smedley

Citation: APL Materials **5**, 116104 (2017); doi: 10.1063/1.5010950
View online: https://doi.org/10.1063/1.5010950
View Table of Contents: http://aip.scitation.org/toc/apm/5/11
Published by the American Institute of Physics

Articles you may be interested in

Direct observation of bi-alkali antimonide photocathodes growth via in operando x-ray diffraction studies
APL Materials **2**, 121101 (2014); 10.1063/1.4902544

Bi-alkali antimonide photocathode growth: An X-ray diffraction study
Journal of Applied Physics **120**, 035303 (2016); 10.1063/1.4959218

Bi-alkali antimonide photocathodes for high brightness accelerators
APL Materials **1**, 032119 (2013); 10.1063/1.4821625

In-situ synchrotron x-ray characterization of K_2CsSb photocathode grown by ternary co-evaporation
Journal of Applied Physics **121**, 055305 (2017); 10.1063/1.4975113

Near atomically smooth alkali antimonide photocathode thin films
Journal of Applied Physics **121**, 044904 (2017); 10.1063/1.4974363

Anisotropic bulk $SmCo_7$ nanocrystalline magnets with high energy product
APL Materials **5**, 116101 (2017); 10.1063/1.4995507

Synthesis and x-ray characterization of sputtered bi-alkali antimonide photocathodes

M. Gaowei,[1,a] Z. Ding,[2] S. Schubert,[3] H. B. Bhandari,[4] J. Sinsheimer,[2] J. Kuehn,[5] V. V. Nagarkar,[4] M. S. J. Marshall,[4] J. Walsh,[1] E. M. Muller,[2] K. Attenkofer,[1] H. J. Frisch,[6] H. Padmore,[3] and J. Smedley[1]
[1]*Brookhaven National Laboratory, Upton, New York 11973, USA*
[2]*Stony Brook University, Stony Brook, New York 11794, USA*
[3]*Lawrence Berkeley National Laboratory, Berkeley, California 94720, USA*
[4]*Radiation Monitoring Devices, Watertown, Massachusetts 02472, USA*
[5]*Helmholtz-Zentrum Berlin, Berlin 12489, Germany*
[6]*University of Chicago, Chicago, Illinois 60637, USA*

(Received 2 February 2017; accepted 20 October 2017; published online 10 November 2017)

Advanced photoinjectors, which are critical to many next generation accelerators, open the door to new ways of material probing, both as injectors for free electron lasers and for ultra-fast electron diffraction. For these applications, the nonuniformity of the electric field near the cathode caused by surface roughness can be the dominant source of beam emittance. Therefore, improving the photocathode roughness while maintaining quantum efficiency is essential to the improvement of beam brightness. In this paper, we report the demonstration of a bi-alkali antimonide photocathode with an order of magnitude improved roughness by sputter deposition from a K_2CsSb sputter target, using *in situ* and *operando* X-ray characterizations. We found that a surface roughness of 0.5 nm for a sputtered photocathode with a final thickness of 42 nm can be achieved while still yielding a quantum efficiency of 3.3% at 530 nm wavelength. © *2017 Author(s). All article content, except where otherwise noted, is licensed under a Creative Commons Attribution (CC BY) license (http://creativecommons.org/licenses/by/4.0/).* https://doi.org/10.1063/1.5010950

Alkali antimonide photocathodes have been the standard option for low visible light photodetectors and image intensifiers for decades. These materials are relatively easy to grow and more resistant against contamination than other options (e.g., Cs:GaAs).[1–4] Recently they have been investigated for use as high-current, low emittance electron sources for next generation accelerator applications such as Linac Coherent Light Source II (LCLS-II).[5] These applications require high quantum efficiency (QE) and long operational lifetime, just as photodetectors do, but also require good correlation of the emitted electrons (e.g., low beam emittance). Unfortunately, while traditional growth methods produce cathodes with a peak quantum efficiency in excess of 30%, these films are very rough and this roughness impacts the beam emittance.[6–8] In this paper, we present results from a bi-alkali antimonide photocathode with an order of magnitude improved surface roughness by sputter deposition from a pre-fabricated K_2CsSb sputter target. A roughness of 0.5 nm for the sputtered cathode has been achieved while yielding sufficient quantum efficiency (QE) (peak QE over 20% at 220 nm and green QE over 3% at 530 nm). The method is controllable and reproducible in film stoichiometry, and the sputter target used for this experiment yields over 25 cathodes without depletion. Film quality is monitored by *in situ* and *operando* X-ray techniques including X-ray fluorescence spectroscopy (XRF), X-ray diffraction (XRD), and X-ray reflectivity (XRR). Detailed post-analysis from these techniques along with the resulting spectral response is also reported. This advancement provides future opportunity for significantly lower emittance photocathodes with equally improved brightness.

[a]Electronic mail: mgaowei@bnl.gov

 © Author(s) 2017

The central enabling advancement is the fabrication of a stoichiometrically controlled alkali antimonide sputter target from which the photocathode was grown. The alkali antimonide sputter target was fabricated at Radiation Monitoring Devices (RMD), Inc. The K_2CsSb compound weighing 10 g was chemically synthesized from the elemental raw materials of cesium, potassium, and antimony. The as-prepared alkali antimonide was sintered into a sputter target format measuring ~48 mm (1.9 in.) in diameter and ~2 mm in thickness, as shown in Fig. 1(a). The target was bonded to a metal backing plate using Nanofoil® (http://www.indium.com/nanofoil/) and subsequently loaded into a Meivac RF sputter gun apparatus located in a self-contained vacuum system with an ion pump and a gate valve to isolate it from the glove box where the target was synthesized. It is important to note that the target was prepared in an inert environment and was loaded into the sputter gun without exposure to ambient moisture or oxygen. The RF sputter gun with the target was shipped in 10^{-9} Torr vacuum to the beamline, where it was attached to the *operando* photocathode growth chamber. The X-ray powder diffraction studies performed on the synthesized compound show the K_2CsSb crystalline cubic phase, as confirmed by ICDD PDF#03-065-4162 in the Joint Committee on Powder Diffraction Standards (JCPDS) and NIST Crystal database. These data have been previously reported.[9]

The cathode growth was carried out in a UHV deposition chamber with the K_2CsSb sputter gun attached. The sputter growth was performed in a noble gas environment (Ar or Ne) with a partial pressure of 20–30 mTorr. The gas passes through an inert gas purifier to reach 10^{-10} Torr partial pressure for water and oxygen. The sputter target was mounted approximately 45° below the sample rotation plane, and when in position, the distance between the target and the substrate was 13 cm. All films were grown using a RF power of 10 W–20 W in order to reach 0.1–0.2 Å/s growth rate for K_2CsSb for better *operando* observation and characterization of the growth process. The target was cleaned by sacrificial sputtering for ~1 h prior to the film growth in order to remove possible degraded surface layer resulting from the transport and installation. Post-cesiation was done by thermal evaporation using cesium getter sources manufactured by SAES. The Cs sources were mounted on a manipulator that could bring the sources perpendicular to the sample normal and ~6.5 cm from the sample surface. The position of the sputter gun and the Cs sources is illustrated in Fig. 1(c).

The *in situ* film growth and real-time characterization were carried out at beamline G3 of the CHESS light-source facility at Cornell University. The incident X-ray beam was 11.3 keV (λ = 1.097 Å) with a photon flux of approximately 10^{14} photons/s which is a relatively high flux enabling fast diffraction scanning and improved signal from off-axis XRR features. The experiments are performed with a beam 0.5 mm wide and 0.75 mm high. The XRR and XRD measurements were carried out using a 4-axis diffractometer with two Pilatus 100 K X-ray cameras mounted downstream for image collection [labeled cam 1 and cam 2 in Fig. 1(c)]. XRR measurements were performed

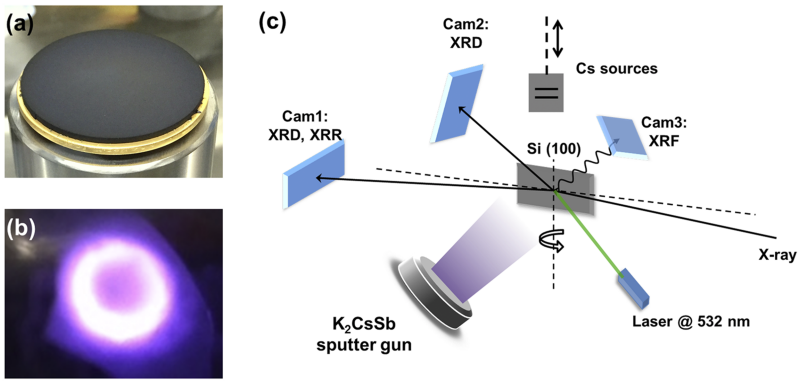

FIG. 1. (a) The K_2CsSb sputter target measuring 1.9 in. (~48 mm) in diameter and ~2 mm thick, bonded to a backing plate. The target was fabricated at RMD, Inc. (b) K_2CsSb sputter target during deposition. (c) Schematic diagram of the *in situ* and *operando* X-ray characterization setup.

by scanning the 2θ angle from 0° to 6°, and XRD measurements were performed by scanning the2θ range from 5° to 30°. During growth, the X-ray beam was kept at a grazing incident angle of 1.4° from the sample surface. Cam 1 was positioned so that the center of the camera was 2.5° with respect to the incident beam in the sample rotation plane and 100 cm away from the sample. Cam 2 was positioned approximately 25 cm from the sample and 45° above the sample rotation plane. An XRF signal was collected by a vortex multi-cathode X-ray detector [labeled cam 3 in Fig. 1(c)] mounted 45° with respect to the sample surface normal and approximately 25 cm away from the sample to measure the stoichiometry during growth. A laser with a wavelength of 532 nm was positioned approximately 25 cm from the cathode surface; the diameter of the laser spot on the surface was about 1 mm with an angle of incidence of 45°. The photocurrent was measured with a Keithley 6517B electrometer. Deposition rates were recorded using an INFICON front load quartz crystal film thickness monitor (QCM).

Substrates used for this experiment were Si(100) wafers cut to 1 cm × 2 cm rectangles. Substrates were ultrasonically cleaned in acetone and isopropanol, followed by hydrofluoric acid (48%) dipping to remove the oxidized layer. Substrates were transferred into the chamber through a vacuum loadlock, heated to 600 °C for 3 h to remove possible surface contamination, and then cooled down to 90 °C for film growth. Chamber base pressure was 1.5×10^{-10} Torr with the major component being N_2/CO (>50%). The partial pressure of both water and oxygen was lower than 10% of the base pressure. During substrate heating, the partial pressure of water rose temporally to 10^{-9} Torr and the total pressure of the chamber was $\sim 5 \times 10^{-9}$ Torr. XRF, XRR, and XRD scans were performed to confirm that the substrate is pristine before growth. A target film thickness of 25 nm of K_2CsSb was sputtered onto the substrates, and samples were further cooled down to 70 °C, followed by Cs deposition in order to maximize the photocurrent at 532 nm. After each growth step, an XRF spectrum was taken to record stoichiometry and θ-2θ scans were taken to determine the crystal structure and texture, film thickness, and roughness. Spectral response was measured for each sample using an optical system which consisted of a Laser Driven Light Source (LDLS) and a Cornerstone monochromator. With this setup, we were able to measure the QE over an incident wavelength ranging from 220 nm to 700 nm (1.77 eV–5.63 eV).

Figure 2(a) shows the XRF spectrum of a cathode grown on a Si(100) substrate. The red curve represents the cathode immediately after sputtering in Ne and the dark curve is the final cathode spectrum after Cs deposition, indicating the relative composition of K, Sb, and Cs. The XRF spectra were analyzed using the software package PyMCA,[10] where the mass concentration for selected elements was calculated from fitting the experimental curve and then normalized to the atomic fractions for K, Sb, and Cs. Elemental mass concentrations for both films are shown in the inset table in Fig. 2(a). From the XRF analysis, we found that the sputter films were rich in Sb and deficient in alkalis compared to the desired K_2CsSb stoichiometry. Such deviation from the stoichiometric ratios can be explained by the combination of non-stoichiometric distribution within the target and different sputter yields for the K, Cs, and Sb elements for current sputter parameters.[11] An excess of Cs in the stoichiometry was observed for the finished cathode compared to the ideal ratio of K:Cs:Sb = 2:1:1, with the final composition being $K_{0.84}Cs_{1.75}Sb$. It has been reported previously that the K–Cs–Sb cathode finished with a cesiation step tended to form a Cs enriched surface termination that has a lower electron affinity at the cathode-vacuum interface.[6]

The XRF spectra for cathodes sputtered in Ar and Ne plasma are compared in Fig. 2(b). Both curves are normalized using the Sb peaks. It is prominent that the Ar sputtered film has a higher alkali/antimony ratio than that of the Ne sputtered photocathode. The inset table in Fig. 2(b) shows that in Ar sputtered films, there are 1.75 alkali atoms per Sb atom, while in the Ne sputtered film, this ratio is 1.24, comparing to an ideal ratio of 3. It is also observed that in the Ar sputtered film the K/Cs ratio is 1.7, while in the Ne sputtered film, this ratio is much closer to the ideal K/Cs ratio of 2. Such a discrepancy can be explained by the different ion bombardment energy carried by single Ar^+ and Ne^+ ions, resulting in different sputter yields for the 2 gases.[11]

The experimental XRR data for each growth step for the same sample along with the fitting results are listed in Fig. 3. Raw data were fitted by GenX based on Parratt's recursion method and Nevot's model, which is widely used for the simulation and fitting of XRR curves of thin films.[12]

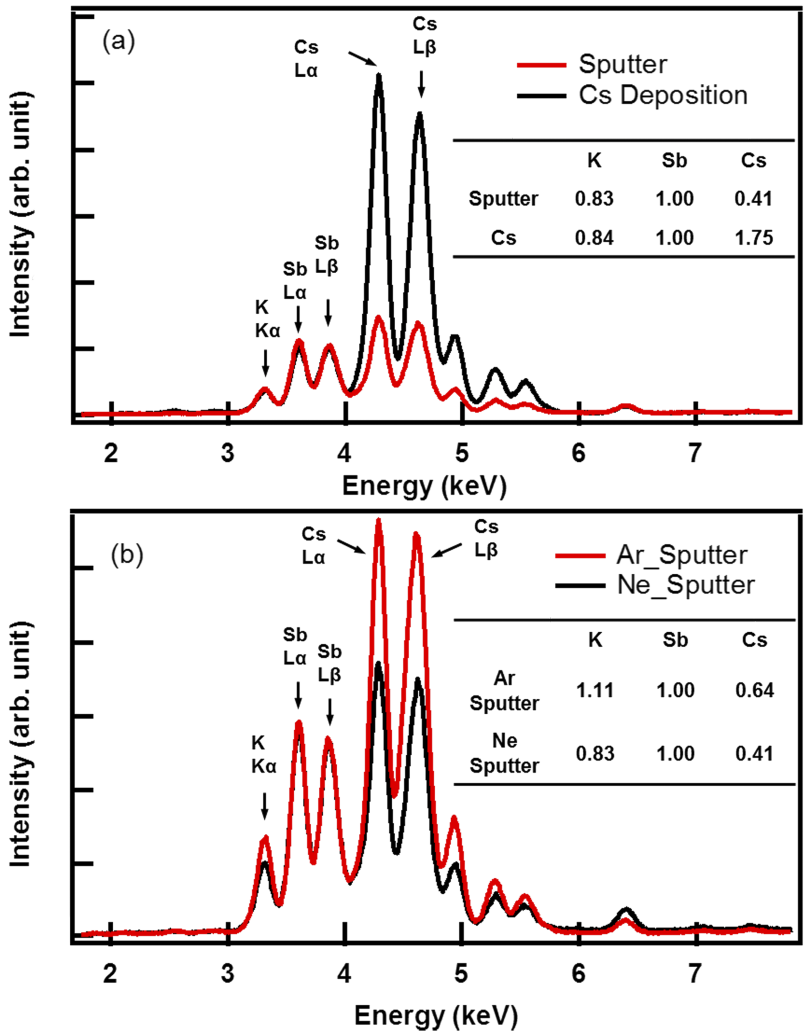

	K	Sb	Cs
Sputter	0.83	1.00	0.41
Cs	0.84	1.00	1.75

	K	Sb	Cs
Ar Sputter	1.11	1.00	0.64
Ne Sputter	0.83	1.00	0.41

FIG. 2. X-ray fluorescence (XRF) spectra of (a) cathode immediately after sputtering in Ne (red) and after Cs deposition (dark); (b) cathode sputtered in Ar (red) and Ne (dark), showing the relative composition of each element. The inset tables present the normalized atomic fraction for each element calculated from curve fitting.

Table I lists the fitted film thickness and surface roughness with uncertainties. The XRR results from the as-sputtered film shows clear oscillations up to 5°. After Cs deposition, oscillations become denser yet still observable up to 3°, indicating a well-maintained surface morphology through the growth process. The fitting of experimental curves yields a rms surface roughness of ~0.52 nm for a 23.4 nm thick sputtered film and ~0.4 nm for the finished photocathode with a final thickness of 41.7 nm. This is remarkably smooth given that the measured roughness is on the order of the unit cell lattice parameter for KCs_2Sb (~0.88 nm).[13] The increased film thickness is a result of lattice expansion on the formation of antimonide from the added Cs reacting with the excess Sb in the sputtered film.[14] The fitting of the oscillations in the sputtered layer mismatches at higher angles, which suggests a variation of film thickness across the sample. This also explains the larger uncertainty in the film thickness estimation. The intrinsic emittance from a similarly smooth alkali antimonide photocathode (roughness 0.6 nm) has been calculated to be 0.14 μm/mm rms at 20 MV/m,[15] which gives an plausible estimation of the emittance from the sputtered cathode in this experiment.

The *in situ* XRD patterns of this sample were compared with simulated powder diffraction patterns calculated using the cubic structure and lattice parameters established in Ref. 13, namely, 8.61 Å for K_2CsSb and 8.88 Å for KCs_2Sb. The missing of diffraction peaks in the XRD scan

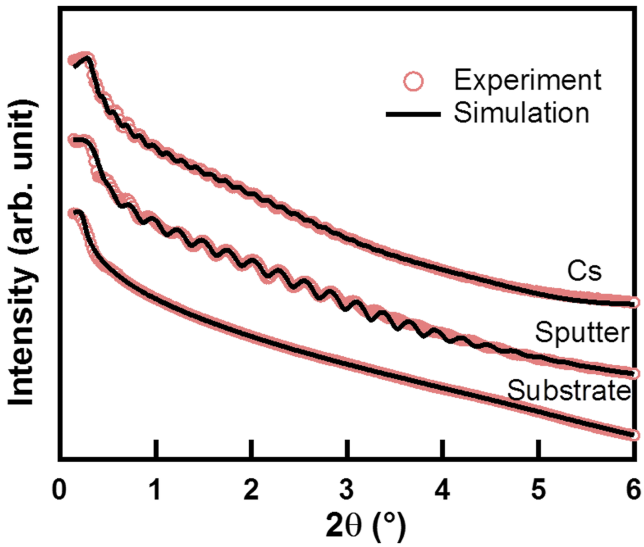

FIG. 3. X-ray reflectivity (XRR) of the sputtered cathode, where the photocathode thickness was ~23 nm, followed by the deposition of Cs. The persistence of oscillations is a testament to the film quality.

in Fig. 4(a) indicates an amorphous structure of the as sputtered layer (~23 nm) under our growth conditions. After Cs deposition, crystallinity was barely observable. The weak peak at $2\theta = 20.16°$ in Fig. 4(a) was identified as the (220) peak of KCs_2Sb (comparing with the calculated value of 20.12°), which also matches the stoichiometry observed in the fluorescence spectrum. A thicker film grown with the same parameters indicated that for a thicker sputtered layer, weak crystallinity can be observed. In Fig. 4(b), the peaks observed at 12.67° and 25.27° for a 49.6 nm sputtered cathode on Si(100) are the (111) and (222) peaks from the cubic phase of K_2CsSb.[16] The appearance of the symmetry-forbidden (111) peak indicates a significant lattice distortion, e.g., weak crystallinity. After adding Cs to this thick sputtered layer, the intensity of the (111) peak dropped significantly, indicating a better formation of the cubic lattice, while the (222) peak shifted towards the lower angle by 0.15°, indicating a slight increase in the lattice constant, a sign of phase transformation from K_2CsSb to KCs_2Sb.

The spectral response measurement between 220 nm and 700 nm for the sputtered cathode is presented in Fig. 5, with a peak QE (at 220 nm) of 23.5% and a QE of 3.3% in the green (530 nm). This growth procedure was repeated several times off the beamline and the QE at 530 nm ranged from 3% to 3.8%. From the evidence based on the XRF and XRD results, we have a reason to believe that the cathodes grown with our method are closer to KCs_2Sb instead of K_2CsSb. The investigation of the electronic structures and the optical properties of these two materials shows that compared to K_2CsSb, KCs_2Sb has a smaller bandgap but a higher absorption of green light (530 nm).[17] Such properties of KCs_2Sb might result in a similar green QE and a lower quantum yield in the UV compared to K_2CsSb photocathodes. A commercial K_2CsSb cathode from Photonis, Inc., was measured in the same geometry and the spectral response (dark curve in Fig. 5) yields in a green QE of 4.6%. The QE difference could rise from the difference in stoichiometry and the rougher surface of cathodes grown

TABLE I. The thickness and surface roughness results of the sputtered cathode and the final cathode after cesiation, compared with a sequentially grown bi-alkali photocathode from Ref. 6.

Sample	Thickness (Å)	Roughness (Å)
Si substrate	N/A	3.27 (−0.03, 0.009)
Sputtered cathode	234.2 (−13.75, 14.47)	5.17 (−0.22, 0.15)
Post-Cs deposition	417 (−13.81, 11.27)	4.19 (−0.08, 0.03)
CsK_2Sb cathode from sequential growth	400–500	250[6]

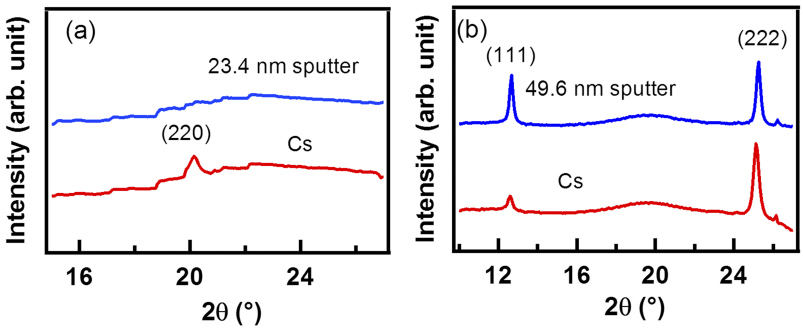

FIG. 4. The XRD spectrum of sputtered layers of thickness (a) 23.4 nm and (b) 49.6 nm, with subsequent cesiation steps. XRD results indicate the amorphous nature of the sputtered cathodes.

sequentially. As discussed previously, this could result in a larger surface area hence higher electron emission current.

In summary, a novel method for creating a low surface roughness photocathode material was presented. Direct sputtering of bi-alkali antimonide photocathodes was prepared by sputter deposition using a pre-synthesized K_2CsSb target. The growth processes were monitored using *in situ* and *operando* XRF, XRR, and XRD measurements to optimize the optical performance of the photocathode. The sputtered bi-alkali cathode material achieved 0.5 nm surface roughness and remained a smooth surface after Cs deposition. With the final cesiation, the cathode reached a sufficient QE of 3.3% in the green. Although the measured green QE of the sputtered cathode was lower than that of sequentially grown K_2CsSb photocathodes, the excellent smooth surface of this cathode will result in an emittance that has much smaller field dependence, which is crucial for future accelerator applications. The composition and the crystal structure in the films can be further improved via optimization of the composition of the target and a better understanding of relative elemental sputter yields. The sputter target we used for this experiment yields over 25 cathodes without depletion. The operation from an already stoichiometric target makes the cathode growth process fast and reproducible. This method may be the optimal method of growing low emittance, ultrasmooth alkali antimonide cathodes in a simple and reproducible manner. As a follow up of this work, there are plans underway to operate a sputtered cathode in a photoinjector to test cathode emittance vs applied field, which is the critically needed data in the community.

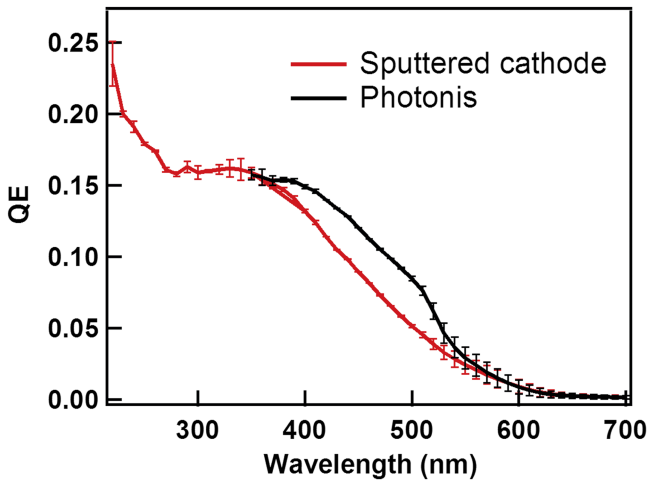

FIG. 5. Quantum efficiencies of a sputtered photocathode on Si(100) substrate (red curve) and a commercial K_2CsSb Photonis photocathode (dark curve). The QE difference could rise from the difference in stoichiometry and the rougher surface (hence a larger surface area) of cathodes grown sequentially, as discussed previously.

The authors would like to thank Arthur Woll, Howie Joress, and beamline staff from Cornell University for their support of our work at CHESS. This work is funded by U.S. Department of Energy, under No. KC0407-ALSJNT-I0013 and SBIR Grant Nos. DE-SC0017202 and DE-SC0017693. The use of CHESS is supported by the NSF and the NIH/NIGMS under NSF Award Nos. DMR-0936384 and DMR-1332208.

[1] P. Michelato *et al.*, "R&D activity on high QE alkali photocathodes for RF guns," in *Proceedings of the 1995 Particle Accelerator Conference* (PAC95 , Dallas, TX, USA, 1995), Vol. 1049.
[2] A. H. Sommer, "Bialkali (K_2CsSb) photocathode as a high-gain secondary-electron emitter," J. Appl. Phys. **43**, 2479–2480 (1972).
[3] T. Rao *et al.*, "Photocathodes for the energy recovery linacs," Nucl. Instrum. Methods Phys. Res., Sect. A **557**, 124–130 (2006).
[4] D. H. Dowell *et al.*, "Cathode R&D for future light sources," Nucl. Instrum. Methods Phys. Res., Sect. A **622**, 685–697 (2010).
[5] B. Dunham *et al.*, "Record high-average current from a high-brightness photoinjector," Appl. Phys. Lett. **102**, 034105 (2013).
[6] S. Schubert *et al.*, "Bi-alkali antimonide photocathodes for high brightness accelerators," APL Mater. **1**, 032119 (2013).
[7] S. Karkare *et al.*, "Effects of surface nonuniformities on the mean transverse energy from photocathodes," Phys. Rev. Appl. **4**, 024015 (2015).
[8] T. Vecchione *et al.*, "Effect of roughness on emittance of potassium cesium antimonide photocathodes," in *Proceeding of the 2012 International Particle Accelerator Conference* (IPAC12, New Orleans, Louisiana, USA, 2012), MOPPP041.
[9] J. Smedley *et al.*, "Sputter growth of alkali antimonide photocathodes: An in operando material analysis," in *Proceeding of the 2015 International Particle Accelerator Conference* (IPAC15, Richmond, VA, USA, 2015), TUPHA003.
[10] V. A. Solé *et al.*, "A multiplatform code for the analysis of energy-dispersive x-ray fluorescence spectra," Spectrochim. Acta, Part B **62**, 63–68 (2007).
[11] N. Laegreid *et al.*, "Sputtering yields of metals for Ar^+ and Ne^+ ions with energies from 50 to 600 eV," J. Appl. Phys. **32**, 365 (1961).
[12] M. Björck *et al.*, "GenX: An extensible x-ray reflectivity refinement program utilizing differential evolution," J. Appl. Crystallogr. **40**, 1174–1178 (2007).
[13] A. R. H. F. Ettema *et al.*, "Electronic structure of Cs_2KSb and K_2CsSb," Phys. Rev. B **66**, 115102 (2002).
[14] J. Xie *et al.*, "Synchrotron x-ray study of a low roughness and high efficiency K_2CsSb photocathode during film growth," J. Phys. D: Appl. Phys. **50**, 205303 (2017).
[15] J. Feng *et al.*, "Near atomically smooth alkali antimonide photocathode thin film," J. Appl. Phys. **121**, 044904 (2017).
[16] M. Ruiz-Oses *et al.*, "Direct observation of bi-alkali antimonide photocathodes growth via in operando x-ray diffraction studies," APL Mater. **2**, 121101 (2014).
[17] L. Kalarasse *et al.*, "Optical properties of the alkali antimonide semiconductors Cs_3Sb, Cs_2KSb, CsK_2Sb, and K_3Sb," J. Phys. Chem. Solids **71**, 314–322 (2010).